Received 2 February 2023, accepted 15 February 2023, date of publication 22 February 2023, date of current version 27 February 2023.

Digital Object Identifier 10.1109/ACCESS.2023.3247604

RESEARCH ARTICLE

Hybrid HMSIW Cavities Antenna With a Half-Pentagon Ring Slot for Bandwidth Enhancement

DIAN WIDI ASTUTI [1], (Member, IEEE), YUYU WAHYU [2], FITRI YULI ZULKIFLI [1], (Senior Member, IEEE), AND EKO TJIPTO RAHARDJO [1], (Member, IEEE)

[1]Department of Electrical Engineering, Universitas Indonesia, Depok 16424, Indonesia
[2]Research Centre for Telecommunications, National Research and Innovation Agency (BRIN), Bandung 40135, Indonesia

Corresponding author: Eko Tjipto Rahardjo (eko@eng.ui.ac.id)

This work was supported by the Publikasi Terindeks Internasional Research Grant-UI (PUTI) 2020 under Contract NKB-646/UN2.RST/HKP.05.00/2020 and Contract NKB-3316/UN2.RST/HKP.05.00/2020.

ABSTRACT A substrate-integrated waveguide (SIW) antenna is an implementation of a waveguide antenna in a microstrip antenna. The microstrip antenna, as a low-profile antenna, suffers from narrow impedance bandwidth. This paper proposes a novel bandwidth enhancement method for solving a narrow impedance bandwidth. Bandwidth enhancement was achieved by using quad-resonant frequencies. The quad-resonant frequencies are resulted from the hybrid half-mode substrate-integrated waveguide (HMSIW) cavities between the inner and outer cavities. The inner HMSIW cavity has a half-pentagon ring slot that disturbs the $TE_{101-\text{inner}}$, $TE_{102-\text{inner}}$, $TE_{202-\text{inner}}$, and $TE_{103-\text{inner}}$ modes, whereas the outer HMSIW cavity consists of two outer quarter-mode substrate-integrated waveguide (QMSIW) cavities. The outer HMSIW cavity generated the $TE_{102-\text{outer}}$ and $TE_{202-\text{outer}}$ modes. The hybrid cavities were fed simultaneously using a port with a quarter-wavelength feed transmission line. The hybrid HMSIW cavities generated resonant frequencies that were close to each other. Additionally, this method was applied to the X-band frequency with a low-profile substrate. The simulated impedance bandwidth and peak realized gain was 33.86% (8.98 – 12.64 GHz) and 7.97 dBi, while the measured impedance bandwidth and peak gain were 31.83% (9.14 – 12.6 GHz) and 7.62 dBi, respectively. Strong agreement was observed between the measurement and simulation results.

INDEX TERMS Bandwidth enhancement, hybrid cavities, quad-resonant, a half-pentagon ring slot, half-mode substrate-integrated waveguide antenna.

I. INTRODUCTION

Substrate-integrated waveguides (SIW) are an attractive technology that offers many advantages, such as high quality, low profile, and the possibility of integrating many components in the same substrate [1], [2], [3]. SIW can be implemented in active and passive components, including antenna elements. One type of SIW implementation in antenna elements involves cavity-backed-slot (CBS) antennas [4]. However, the SIW CBS antenna has a narrow impedance bandwidth (1.7%) owing to its high quality, and its structure is associated with only a single resonant frequency [4]. Various techniques have been employed to improve the impedance bandwidth through slot substrate removal [5], slot radiator modification [6], [7], [8], [9], shorting vias [10], [11], [12], [13], and dual-mode SIW with pin loading [14].

Substrate removal [5] can be implemented to improve the narrow bandwidth by decreasing the slot capacitance of a conventional SIW CBS antenna. A 24% wider bandwidth and 6.2% higher antenna efficiency were achieved using this technique when compared with the conventional SIW CBS antenna. However, the substrate removal method is not an

The associate editor coordinating the review of this manuscript and approving it for publication was Bilal Khawaja.

easy task, and the impedance bandwidth improvement is not significant, because it still has a single resonant frequency.

Slot radiator modifications, such as non-resonant slots [6], dual unequal slots [7], bowtie slots [8], and dumbbell slots [9], can be implemented to improve the narrow impedance bandwidth by resulting in hybrid-, triple-, and penta-resonant frequencies. Penta-resonant frequencies successfully enhance impedance bandwidth by up to 26.7% [9]. Penta-resonant frequencies were successfully generated by even and odd high-order modes, tilted slots of the feeding structure, and a combination of two high-order modes. However, these antenna dimensions [6], [7], [8], [9] are large owing to their full-mode SIW (FMSIW) structure.

An investigation of the via hole above the slot [10] yielded an impedance bandwidth of 3.35 %. A pair of shorting vias was used to combine the lower cavity mode with the higher modes [11] and 17.5% of impedance bandwidth has developed. Another method of combining a pair of shorting vias with a cross-shaped slot can be used to improve the impedance bandwidth by generating multi resonant frequencies [12], [13]. Multi resonant frequencies consist of even- and odd-high-order modes. Multi resonant frequencies, that is, triple- [11], [11], [12], penta- [12], [13], and hepta- [13] resonant frequencies, successfully yielded improvements in the impedance bandwidth. Hepta-resonant frequencies in an elliptical cavity improve impedance bandwidth by up to 22.7% [13]. However, shortening the placement of the vias is difficult. Another bandwidth enhancement method can be achieved using aperture coupling of the patch antenna. The patch antenna was fed using dual-mode SIW [14]. A 22% impedance bandwidth was achieved using triple-resonant frequencies with a stack substrate. However, the alignment of the stack substrates is not an easy task.

A SIW also offers miniaturization by dividing a single cavity into sub-cavities, such as the HMSIW, QMSIW, and eighth-mode SIW (EMSIW), because the dominant mode field distributions of these cavities are similar. This can be implemented using multiplexed antennas [15], [16], [17], [18]. However, multiplexing antennas [15], [16], [17], [18] and HMSIW CBS antennas with single resonant frequencies [19], [20] have narrow impedance bandwidths. The impedance bandwidths are not more than 5%. Few studies have focused on improving the impedance bandwidth in sub-cavities SIW antennas, such as in the cavities of HMSIW, QMSIW, and EMSIW, using slot modification [21], [22], [23], coupling [24], [25], [26], fraction modes [27], and metamaterials [28]. Impedance bandwidth improvements of up to 23.7% were realized through hybrid-resonant frequencies in the HMSIW cavity [28]. However, owing to the limited patch area of a single HMSIW cavity [21], [22], [23] and the use of substrates with a high profile thickness [28], only triple resonant frequencies have been reported [22].

In this study, a novel method using hybrid HMSIW cavities between the inner and outer cavities was proposed for bandwidth enhancement. The inner and outer HMSIW cavities have different dimensions; the outer HMSIW cavity has larger dimensions than the inner HMSIW cavity. The inner and outer HMSIW cavities are fed simultaneously to generate a series of resonant frequencies. The series of resonant frequencies are close to each other and merge. The inner HMSIW cavity uses a half-pentagon ring slot to excite the triple-resonant frequencies, whereas the addition of an outer HMSIW cavity improves the impedance bandwidth. To the best of our knowledge, this is the novelty of impedance bandwidth enhancement. This study is also an improvement over previous research [23], where hybrid resonant frequencies were used for impedance bandwidth enhancement.

TABLE 1. Dimension of ant-3 design (unit = mm).

Parameter	*Wsub*	*Lsub*	*Wcop*	*Lcop*	*Dv*
Value	18.5	45	14	25	1
Parameter	*Pv*	*Lv*	*Wf*	*Lf*	*Hs*
Value	1.5	4.46	2.43	5	9.1
Parameter	*St*	*Ls*	*h*	*Lc*	*Wc*
Value	0.6	20.42	1.575	16.55	16.55

The main contributions of this paper are:

1) A novel bandwidth-enhancement method was developed using quad-resonant frequencies with hybrid HMSIW cavities between the inner and outer cavities. This resulted in an impedance bandwidth measurement of 31.83% (9.14 – 12.6 GHz).
2) Simple structure using a half-pentagon ring slot on the inner and outer HMSIW cavities without additional substrates
3) A low-profile SIW antenna with 0.048 λ_0 at 9.14 GHz, and
4) 50% miniaturized the SIW CBS antenna that used the HMSIW structure.

II. DESIGNED ANTENNA AND PARAMETRIC STUDY

The geometry of the proposed antenna, Ant-3, is shown in Fig. 1. Ant-3 has hybrid HMSIW cavities with a half-pentagon ring slot in the inner HMSIW cavity for impedance bandwidth enhancement. A Rogers-Duroid 5880 substrate with a thickness (h) of 1.575 mm, dielectric relative permittivity (ε_r) of 2.2, and tangent loss (δ) of 0.0009 was used for the proposed antenna and fabrication. The proposed antenna is simulated using an electromagnetic full-wave simulator. The antenna dimensions are listed in Table. 1.

The impedance bandwidth enhancement of Ant-3 is resulted from the evolution of the hybrid HMSIW cavities antenna, as shown in Fig. 2. The proposed antenna begins with a basic cavity antenna. The basic cavity antenna consists of an inner FMSIW cavity and a fourth outer sub-cavities (QMSIW), as shown in Fig. 2(a). The inner and outer cavities were separated diagonally using holes. Each via hole has diameter D_v, distance between two adjacent hole centers (P_v), and free-space wavelength (λ_0). The separation can be optimized to minimize the energy leakage [29]. Therefore,

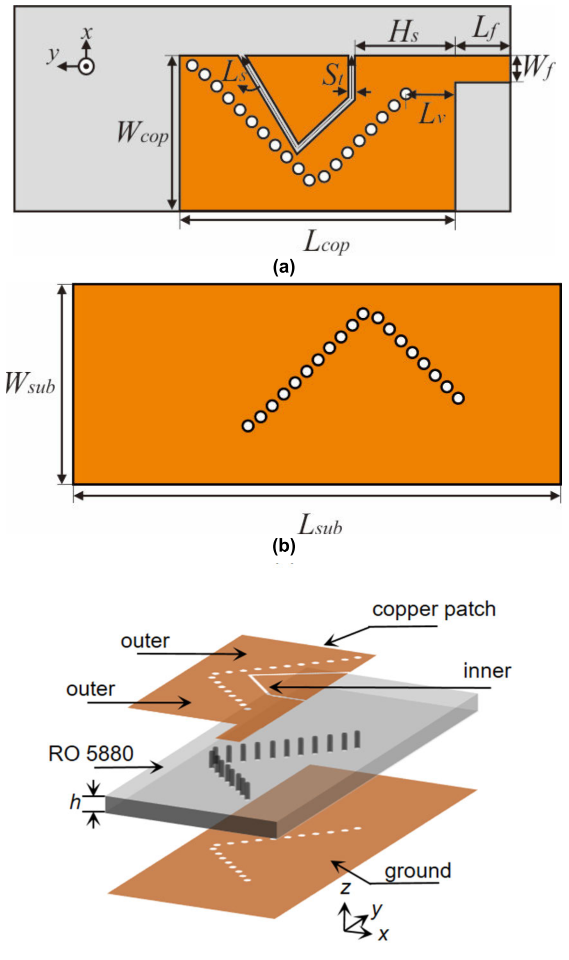

FIGURE 1. The geometry of hybrid half-mode substrate-integrated waveguide (HMSIW) cavities antenna Ant-3 design. The antenna dimensions are listed in Table 1. (a) Copper patch details, (b) ground details, and (c) 3-D detail.

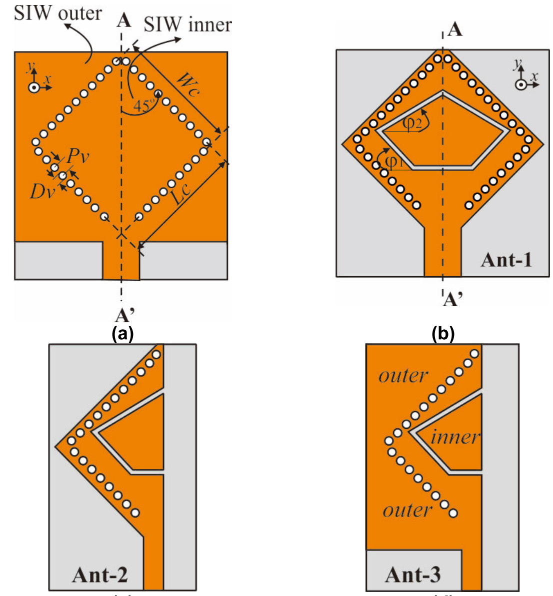

FIGURE 2. Evolution of hybrid half-mode substrate-integrated waveguide (HMSIW) cavities antenna with half-pentagon ring slot: (a) the basic cavities for the inner and the outer, (b) Ant-1, (c) Ant-2, and (d) Ant-3.

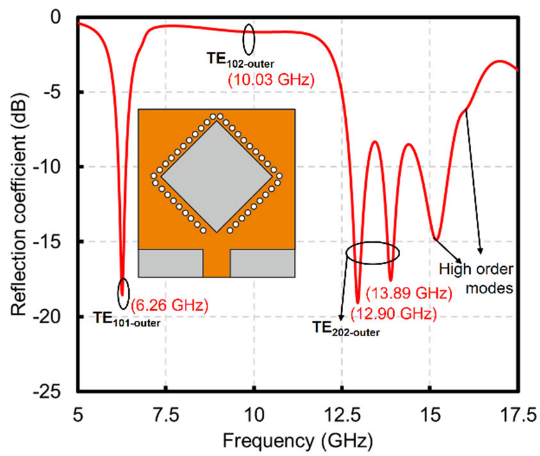

FIGURE 3. Reflection coefficient simulation for the fourth outer sub-cavities QMSIW.

TABLE 2. The calculated series of TE modes for outer QMSIWs (GHz).

m \ p	1	2	3	4	5
1	6.271	9.916	14.023	18.284	22.611
2		12.543	15.989	19.832	23.880
3			18.814	22.172	25.857
4				25.085	28.394
5					31.356

$D_v/P_v \geq 0.5$ and $\lambda_0/D_v \geq 10$ should be considered for this optimization.

The inner and outer cavity dimensions were influenced by the frequency implementation. In the proposed antenna, the X-band frequency range was used for the frequency implementation in the $TE_{102-\text{outer}}$ mode. The inner FMSIW cavity dimensions were obtained by determining the $TE_{102-\text{outer}}$ mode as the frequency implementation, as indicated by the *Lc*-inner and *Wc*-inner dimensions. The outer and inner cavities were fed simultaneously by using 50 Ω characteristic impedances and a quarter-wavelength feed transmission line. The calculated series of resonant frequencies were determined by the four outer sub-cavities, QMSIW, as listed in Table 2, and the inner FMSIW cavities, as listed in Table. 3. The TE modes of the resonant frequencies were calculated based on [30].

The TE modes of the fourth outer sub-cavities, QMSIW, were simulated using ANSYS HFSS, as shown in Fig. 3. The predicted resonances for the $TE_{101-\text{outer}}$, $TE_{102-\text{outer}}$, and $TE_{202-\text{outer}}$ modes were excited at 6.26, 10.03, and 12.90 GHz, respectively. These predictions matched the results of the calculations presented in Table 2. The same prediction is made for the inner FMSIW cavity. According

TABLE 3. The calculated series of TE modes for inner FMSIW (GHz).

m \ p	1	2	3	4	5
1	8.985	14.207	20.092	26.197	32.397
2		17.971	22.908	28.414	34.215
3			26.956	31.768	37.048
4				35.941	40.683
5					44.927

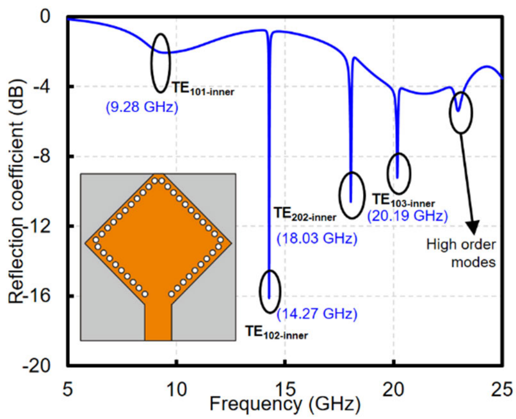

FIGURE 4. Reflection coefficient simulation for the inner FMSIW cavity.

to Fig. 4, which shows these frequencies, the expected resonances for the $TE_{101-\mathrm{inner}}$, $TE_{102-\mathrm{inner}}$, $TE_{202-\mathrm{inner}}$, and $TE_{103-\mathrm{inner}}$ modes were excited at 9.28, 14.27, 18.03, and 20.19 GHz, respectively. These predictions match the results of the calculations presented in Table 3 for these modes.

The four outer sub-cavities, QMSIW, of the basic cavity antenna were removed, and the antenna became a conventional antenna with a single FMSIW cavity, named Ant-1, as shown in Fig. 2(b). Ant-1 uses a pentagon ring slot as the radiating slot in its inner FMSIW cavity. Ant-1 had a pentagon ring slot shape consisting of three segments: horizontal, right-slanted, and left-slanted. Right-slanted and left-slanted segment ring slots occurred at $\phi_1 = -47°$ and $\phi_2 = 31°$, respectively. The half-pentagon ring slot segment has an approximate ratio of 1:2:3 based on the guided wavelength of the $TE_{102-\mathrm{outer}}$ mode.

Ant-1 generates a resonant frequency on the $TE_{102-\mathrm{inner}}$ mode and Ant-1 can be operated on 11.61 – 11.81 GHz (1.71%) associated with the −10 dB reflection coefficient as indicated in Fig. 5. Ant-1 suffers from narrow bandwidth and large dimensions. A narrow bandwidth occurs because of the single resonant frequency, whereas a large dimension occurs because of the use of the FMSIW structure. Ant-1 can be minimized by dividing it vertically along the AA' line. Ant-1 becomes two parts of Ant-2, as shown in Fig. 2(c). Each part of Ant-2 is an HMSIW CBS antenna with a 50% miniaturization from the FMSIW CBS structure.

Ant-2 can generate triple resonant frequencies, which are combinations of $TE_{101-\mathrm{inner}}$, $TE_{102-\mathrm{inner}}$, and $TE_{202-\mathrm{inner}}$

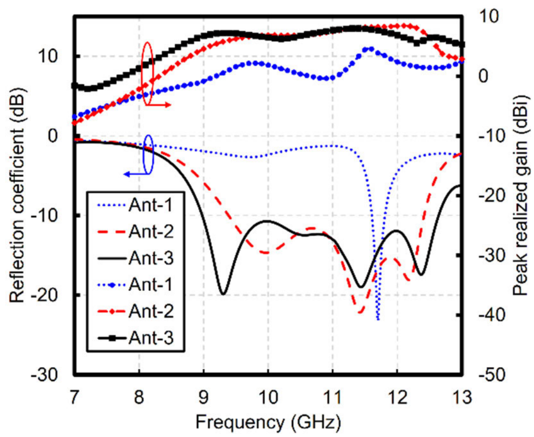

FIGURE 5. Reflection coefficient simulation for antenna evolution of hybrid half-mode substrate-integrated waveguide (HMSIW) cavities.

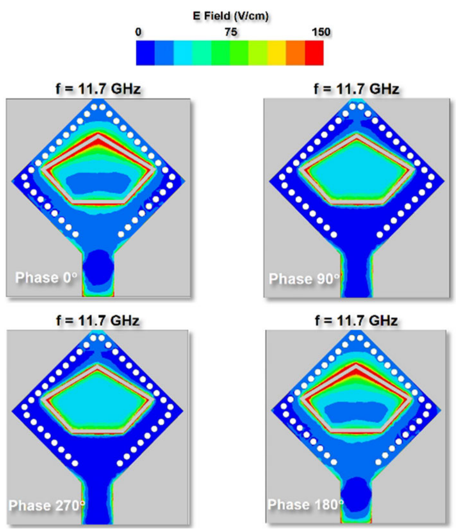

FIGURE 6. Electric field distribution Ant-1 at 11.7 GHz on phase 0°, 90°, 180°, and 270°.

modes. The impedance bandwidth significantly improved to 27.71% (9.39 – 12.41 GHz). The additional outer part of Ant-2 results in the Ant-3 design, as shown in Fig. 2(d). The combination of the inner and outer HMSIW cavities (Ant-3) resulted in quad-resonant frequencies. These frequencies are associated with an impedance bandwidth of 33.86% (8.98 – 12.64 GHz), indicating that the outer HMSIW improved the impedance bandwidth.

Fig. 5 shows a comparison of the peak realized gain for the antenna evolution. Ant-1 has a maximum 4.56 dBi peak realized gain at 11.6 GHz. The peak realized gain is 3.86 dBi on 11.7 GHz. The peak realized gain for Ant-1 fluctuates significantly. The peak realized gains for Ant-2 and Ant-3 are flatter than those for Ant-1. The peak realized gains for Ant-2 and Ant-3 are higher than those for Ant-1. The peak realized gain for Ant-2 raises from 6 dBi up to 8.44 dBi in the range 9.39 – 12.1 GHz and declines to 7.32 dBi in the range 12.1 – 12.41 GHz. In the impedance bandwidth range

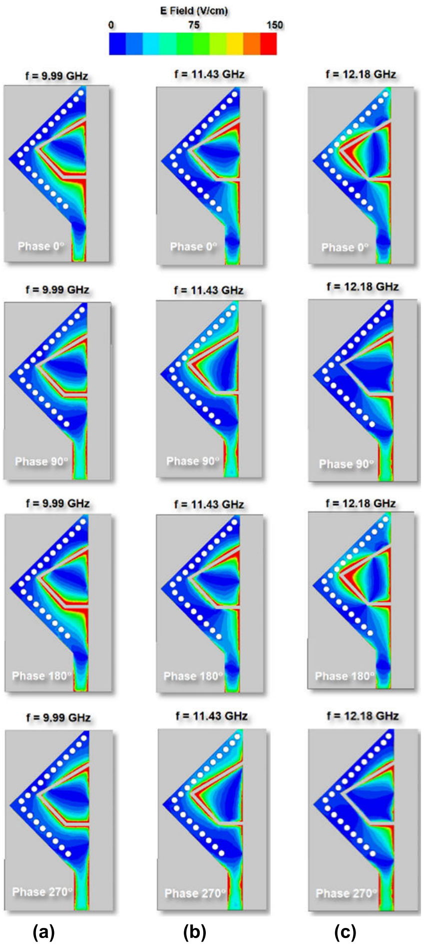

FIGURE 7. Electric field distribution Ant-2 at (a) 9.99, (b) 11.43, and (c) 12.18 GHz on phase 0°, 90°, 180°, and 270°.

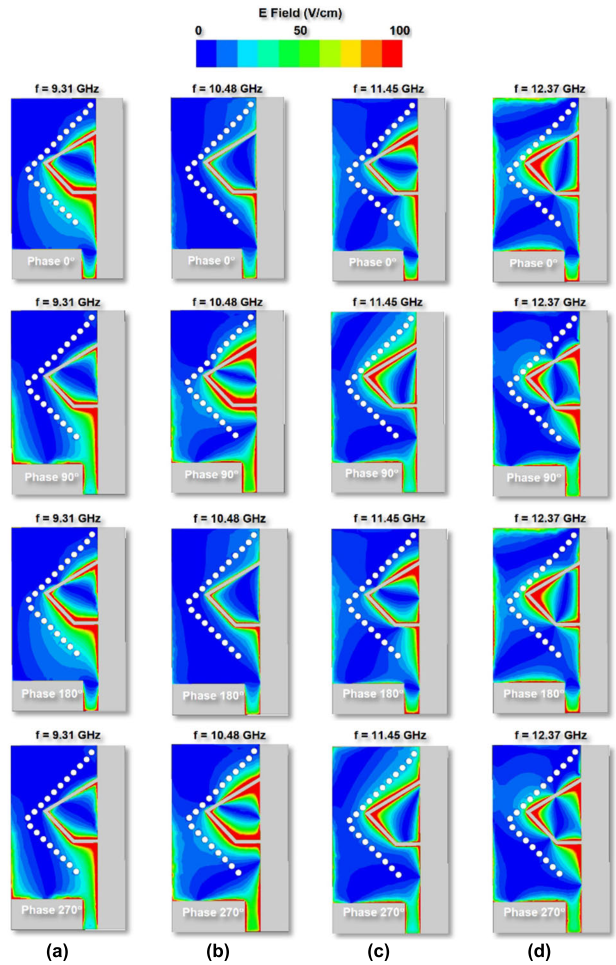

FIGURE 8. Electric field distribution Ant-3 at (a) 9.31, (b) 10.48, (c) 11.45, and (d) 12.37 GHz on phase 0°, 90°, 180°, and 270°.

(8.98 – 12.64 GHz), Ant-3 has a minimum of 5.53 dBi at 12.3 GHz and a maximum of 7.97 dBi at 11.4 GHz for the peak realized gain. The flatter peak realized gains on Ant-2 and Ant-3 occur because of the combination of TE modes that merged, rather than on Ant-1, which has a single TE mode.

A. ANALYSIS OF ELECTRIC FIELD MODE

An analysis of the electric field distribution was performed to understand the TE modes that combine and radiate into the free air. The Ant-1 and Ant-2 structures consisted of copper patch resonators located in the inner cavity. Therefore, the modes merging from the single- to triple-resonant frequencies originated only from this cavity. The electric field distribution for Ant-1 occurs at 11.7 GHz as shown in Fig. 6. The electric field distribution for Ant-1 had the same scale of 150 V/cm for one period for each phase 90° increment. The electric field distribution of Ant-1 occurs because of the strong $TE_{101-\text{inner}}$ and weak $TE_{102-\text{inner}}$ mode combinations.

Fig. 7 shows the electric field distribution of Ant-2 at 9.99, 11.43, and 12.18 GHz on the same scale of 150 V/cm. The electric field distribution at 9.99 GHz occurs because of the strong $TE_{101-\text{inner}}$ and weak $TE_{102-\text{inner}}$ mode combination. This is demonstrated by the same electric field distribution for each phase increment, as shown in Fig. 7(a). Fig. 7(b) shows the electric field distribution at 11.43 GHz and which occurs because of the $TE_{202-\text{inner}-\text{odd}}$ mode. This is proven by the different 90° phases in one period. While in Fig. 7(c) shows the electric-field distribution for the $TE_{202-\text{inner}-\text{even}}$ mode.

Ant-3 consists of an inner HMSIW resonator and outer HMSIW resonator. The outer HMSIW consists of both outer QMSIW cavities, and the QMSIW cavity can generate $TE_{102-\text{outer}}$ and $TE_{202-\text{outer}}$ modes. The quad-resonant frequencies resulted in bandwidth enhancements of 9.31, 10.48, 11.45, and 12.37 GHz. Through reflection coefficient simulations based on antenna evolution (see Fig. 5), these frequencies can be easily defined as combinations of $TE_{101-\text{inner}}$, $TE_{102-\text{inner}}$, $TE_{202-\text{inner}}$, $TE_{103-\text{inner}}$, $TE_{102-\text{outer}}$, and $TE_{202-\text{outer}}$.

Fig. 8 shows the electric field distribution at the same scale as the 100 V/cm electric field distribution. The electric field distribution in the inner HMSIW is stronger than that in the outer HMSIW. Fig. 8(a) shows the first of electric-field distribution at 9.31 GHz. The maximum electric field distribution in the inner HMSIW occurred along

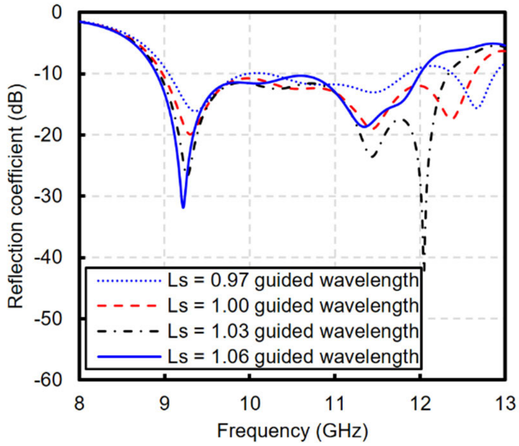

FIGURE 9. Reflection coefficient simulation for Ls parameter as a half-pentagon ring slot length.

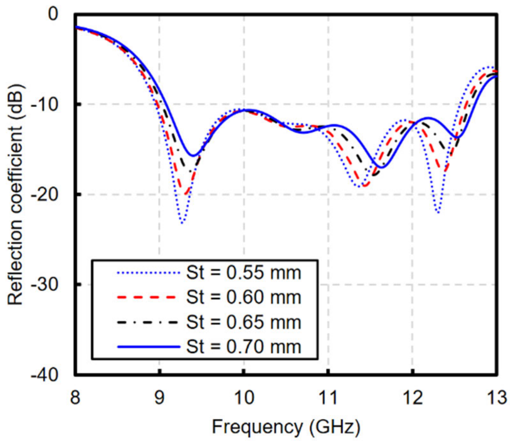

FIGURE 10. Reflection coefficient simulation for St parameter as a half-pentagon ring slot thickness.

the horizontal, right, and left slant half-pentagon ring slot segments. In the inner HMSIW, the distribution is resulted from the strong $TE_{101-inner}$ and weak $TE_{102-inner}$ modes in the same phase. The electric field distribution in the outer HMSIW resulted from the $TE_{102-outer}$ mode.

The second quad-resonant frequencies was located at 10.48 GHz as shown in Fig. 8(b). The maximum electric field distribution occurred in the upper and lower parts of the half-pentagon ring slots in the inner HMSIW. The distribution also occurred in the outer HMSIW, similar to that in the $TE_{102-outer}$ mode. In the inner HMSIW, the electric field distribution was induced by a combination of the strong $TE_{102-inner}$ and weak $TE_{101-inner}$ modes. This indicates that the inner HMSIW had a different phase.

The third resonant frequency occurs at 11.45 GHz as shown in Fig. 8(c). The maximum electric field distribution in the inner HMSIW occurred on the left slant half-pentagon ring slot segment and inner edge of the cutting magnetic wall. This was attributed to the $TE_{202-inner-odd}$ mode. The electric field on the outer HMSIW was identified as $TE_{202-outer-odd}$ mode.

The last resonant frequency is located at 12.37 GHz as shown in Fig. 8(d). The electric field distribution on the inner HMSIW occurs because of the combination of the weak $TE_{202-inner-even}$ and the strong $TE_{103-inner}$ modes, while on the outer HMSIW results by the $TE_{202-outer-even}$ mode.

B. PARAMETRIC ANALYSIS OF BANDWIDTH ENHANCEMENT

Parametric analyses were performed to verify the impedance bandwidth enhancement in the inner and outer HMSIW cavities. Generally, impedance bandwidth enhancement is influenced by the length and width of a half-pentagon ring slot. This was also influenced by the position of the half-pentagon ring slot relative to the bottom edge of the copper patch.

A half-pentagon ring slot with approximately one guided wavelength $TE_{102-outer}$ mode was added to the top substrate. The slot shape has an asymmetric segment that disrupts the electric-field distribution of the $TE_{101-inner}$, $TE_{102-inner}$, $TE_{202-inner}$, and $TE_{103-inner}$ modes. The two outer QMSIWs contributed to the electric field distribution of the $TE_{102-outer}$ and $TE_{202-outer}$ modes.

Fig. 9 shows the reflection coefficient simulation for a half-pentagon ring slot length, Ls. The impedance bandwidth was 33.86% when $Ls = 1.00$ times the guided wavelength of the $TE_{102-outer}$ mode. If this length is larger than the guided wavelength of the $TE_{102-outer}$ mode, quad-resonant frequencies still exist, but the impedance bandwidth is narrow. For example, when $Ls = 1.03$ times the guided wavelength of the $TE_{102-outer}$ mode, the proposed antenna can operate at $8.94 - 12.34$ GHz. This implies that the proposed antenna has an impedance bandwidth of 31.95 %. When $Ls = 1.06$ times the guided wavelength of the $TE_{102-outer}$ mode, the proposed antenna has an impedance bandwidth of 29.56% ($8.91 - 12.00$ GHz). The fourth resonant frequency separates the frequency bands, and the quad-resonant frequencies become triple-resonant frequencies. This occurs when the length of the half-pentagon ring slot is smaller than that of the guided-wavelength $TE_{102-outer}$ mode ($Ls = 0.97$). The proposed antenna had a 26.88% impedance bandwidth of $9.05 - 11.86$ GHz.

The half-pentagon ring slot thickness also influences the impedance bandwidth improvement, as shown in Fig. 10. The proposed antenna has a maximum impedance bandwidth when the slot thickness is $St = 0.6$ mm. Quad-resonant frequencies can still be achieved for other slot thickness parameters even though the impedance bandwidth is narrow. For example, when $St = 0.55$ mm, the proposed antenna has a 33.64% impedance bandwidth that can be implemented at 8.95 – 12.57 GHz. The narrow impedance bandwidth also occurs when the slot thickness $St = 0.65$ and $St = 0.70$ mm with 33.63% (9.03 – 12.68 GHz) and 33.55% (9.08 – 12.74 GHz). With increasing thickness of the half-pentagon ring slot, the quad-resonant frequencies shifted to a higher frequency, and the reflection coefficient values increased.

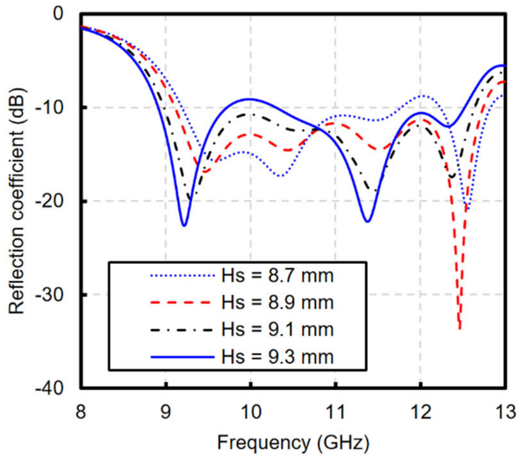

FIGURE 11. Reflection coefficient simulation for Hs parameter as a half-pentagon ring slot position.

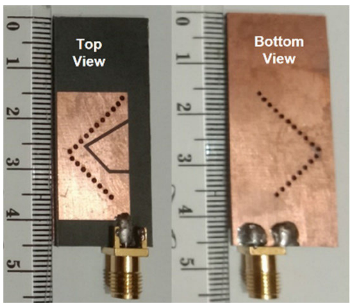

FIGURE 12. The photo of the antenna fabrication.

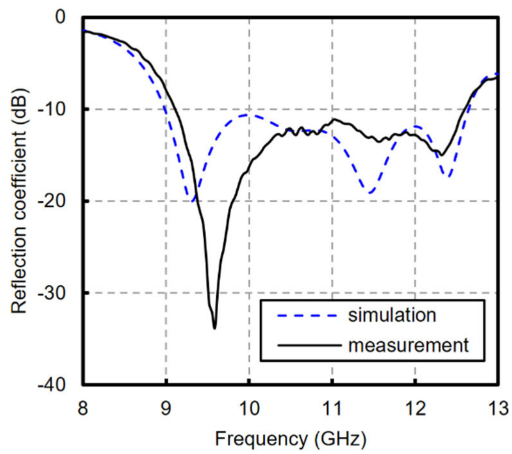

FIGURE 13. Reflection coefficient simulation and measurement of the proposed antenna.

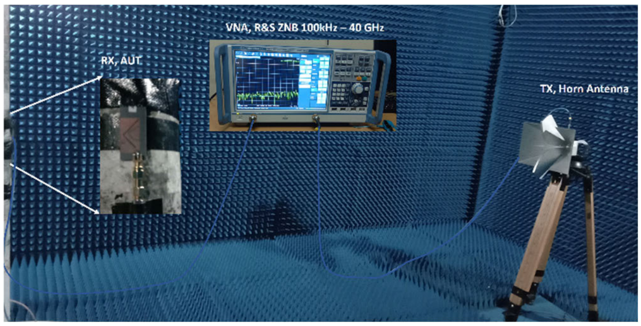

FIGURE 14. Measurement of the peak gain and radiation pattern of the proposed antenna.

The half-pentagon ring-slot position starts at the end of the feed transmission line and has a considerable influence on the quad-resonant frequencies, as shown in Fig. 11. When a half-pentagon ring slot was placed near the upper sidewall, most of the quad-resonant frequencies shifted to lower resonant frequencies, with the exception of the second resonant frequency. The quad-resonant frequencies combination for the broadband range was achieved when the half-pentagon slot was not placed above or below the upper sidewall. For example, when $Hs = 9.3$ mm, the first quad-resonant frequencies separate and become dual-band frequencies. The first resonant frequency had an 8.7% (8.91 – 9.72 GHz) impedance bandwidth, whereas the other triple resonant frequencies had an impedance bandwidth of 19.55% (10.29 – 12.52 GHz). The same conditions were applied for $Hs = 8.7$ mm. Triple resonant frequencies have 24.62% (9.19 – 11.77 GHz) impedance bandwidth and the fourth resonant frequencies has 4.79% (12.23 – 12.83 GHz) impedance bandwidth. Quad-resonant frequencies have the maximum impedance bandwidth on $Hs = 8.9$ mm and $Hs = 9.1$ mm with impedance bandwidths of 33.23% and 33.86%, respectively.

From the above impedance bandwidth enhancement method (Ant-3), the following steps can be implemented in other frequency-band applications:

1) Set the frequency center as the $TE_{102-\text{outer}}$ mode on a substrate with a dielectric relative permittivity (ε_r) of 2.2, tangent loss (δ) of 0.0009, and thickness (h) of 1.575 mm,
2) Calculate the outer and inner HMSIW cavities dimensions according to [30] for all the TE modes.
3) Add the 50 Ω width and quarter-wavelength of the $TE_{102-\text{outer}}$ mode as the feed transmission line.
4) Put one of the guided wavelengths of the $TE_{102-\text{outer}}$ mode as a half-pentagon ring slot with a ratio of 1:2:3 for the horizontal, right-slanted, and left-slanted segments. The right-slanted and left-slanted segments were set as $\phi_1 = -47^\circ$ and $\phi_2 = 31^\circ$, respectively.
5) Optimize the guided wavelength, thickness, and position of the half-pentagon ring slot and the width feed transmission line for impedance bandwidth improvement by resulting in quad-resonant frequencies.

III. RESULT AND DISCUSSION

The proposed antenna was fabricated using a photo etching process, as shown in Fig. 12. The fabricated antenna was validated by measurements to verify the impedance bandwidth enhancement method, as shown in Fig. 13. The measured and simulated impedance bandwidths for the −10 dB reflection coefficient are 3.46 GHz (9.14 – 12.6 GHz) and 3.66 GHz

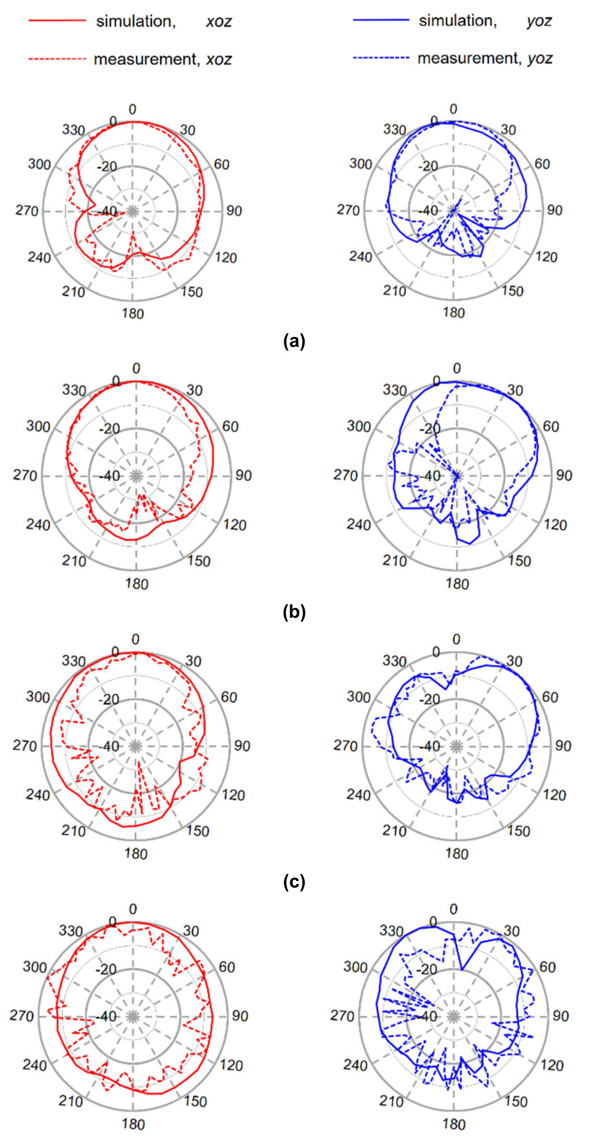

FIGURE 15. The radiation pattern was simulated and measured for quad-resonant frequencies on (a) 9.33 GHz, (b) 10.5 GHz, (c) 11.5 GHz, and (d) 12.32 GHz.

(8.98 – 12.64 GHz), respectively. The measured impedance bandwidth deviates only modestly from the measured value, possibly owing to the fabrication of the antenna and the soldering connector.

Fig. 14 shows the anechoic chamber room used for the radiation pattern measurement. The radiation pattern measurement used a standard method that employed a VNA as the signal generator, a spectrum analyzer, and a horn antenna. The signal generator from the VNA radiates electromagnetic waves into the air using a horn antenna, and the antenna under test (AUT) receives electromagnetic waves. The far-field condition must be considered for the radiation pattern measurement, including the alignment between the AUT and horn antenna, to obtain a better radiation pattern and peak gain.

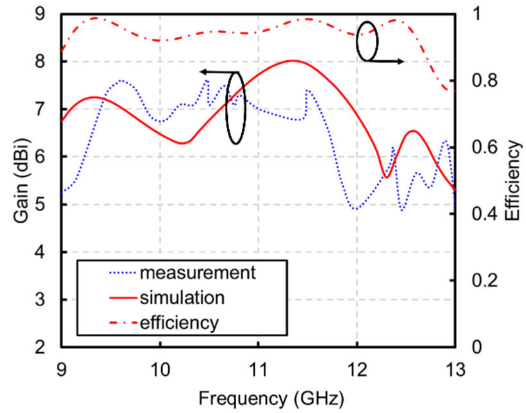

FIGURE 16. Peak gain simulation and measurement of the proposed antenna.

TABLE 4. Comparison of proposed measured antenna with previously published studies.

Ref	Type	Res.	Dimensions (λ_0^3)	Max. gain (dBi)	FBW (%)
[9]	dumbbell slot	penta	1.21×1.10×0.05	9.5	26.7
[12]	cross slot + shorting vias	penta	0.98×0.59×0.03	5.72	20.8
[13]	ellips cavity, cross slot + shorting vias	hepta	1.17×0.81×0.03	7.4	22.7
[14]	dual mode + pin loaded	triple	0.63×0.59×0.08	11.8	21
[22]	epsilon shaped slot	triple	0.81×0.56×0.03	6.7	13.2
[23]	triangular slot	hybrid	0.38×0.38×0.02	4.2	9.87
This work	**hybrid HMSIW**	**quad**	**0.76×0.43×0.05**	**7.62**	**31.83**

λ_0 : The wavelength in the free space for the lowest frequency.

Fig. 15 shows the normalized radiation pattern simulation and measurement for quad-resonant frequencies of 9.33, 10.5, 11.5, and 12.32 GHz. Omnidirectional and unidirectional radiation patterns were observed for the *xoz* and *yoz* cut planes, with a main beam direction of 30°. The radiation patterns obtained from the simulation and measurement results were similar for both the planes, although a discrepancy was observed in the main beam direction. This results from the inner HMSIW cavity and electric field distribution on a half-pentagon ring slot, as shown in Fig. 8.

The simulated and measured gain values are shown in Fig. 16. The simulated peak realized gain is 7.96 dBi. The measured value fluctuates between 5 dBi and 7.62 dBi, owing to the measurement conditions in the anechoic chamber and the effect of different mode combinations. The simulated efficiency, which ranges from 0.90 to 0.97, is shown in Fig 16.

Table 4 presents the proposed antenna results, which were compared with those of previously published studies. Hybrid HMSIW cavities with quad-resonant frequencies significantly increased the impedance bandwidth. The proposed antenna has a broadband impedance of up to 31.83%, which is larger than those of other SIW cavity-slot antennas. Furthermore, the outer HMSIW resonator succeeded in adding another resonance without a substrate extension. The proposed antenna also has a higher gain than those in [22] and [23] for the HMSIW structures.

IV. CONCLUSION

A novel hybrid HMSIW cavities antenna with a half-pentagon ring slot was investigated, fabricated, and tested for impedance bandwidth enhancement. Impedance bandwidth enhancement was achieved using hybrid HMSIW cavities between the inner and outer cavities. The inner HMSIW cavity used a half-pentagon ring slot. This method results in quad-resonant frequencies consisting of the $TE_{101-\text{inner}}$, $TE_{102-\text{inner}}$, $TE_{202-\text{inner}}$, $TE_{202-\text{outer}}$, and $TE_{103-\text{outer}}$ mode combinations. The implementation of the X-band frequency range application yielded a measured impedance bandwidth of 31.83% (9.14 –12.6 GHz). The flat gain achieved ranged from 5 dBi to 7.62 dBi with a unidirectional radiation pattern obtained for the *yoz* cut plane.

REFERENCES

[1] M. Bozzi, A. Georgiadis, and K. Wu, ''Review of substrate-integrated waveguide circuits and antennas,'' *IET Microw., Antennas Propag.*, vol. 5, no. 8, pp. 909–920, Jun. 2011.

[2] K. K. Samanta, D. Stephens, and I. D. Robertson, ''Design and performance of a 60-GHz multi-chip module receiver employing substrate integrated waveguides,'' *IET Microw., Antennas Propag.*, vol. 1, no. 5, pp. 961–967, Oct. 2007.

[3] T. Djerafi, K. Wu, and A. Doghri, ''Substrate integrated waveguide antennas,'' in *Handbook of Antenna Technologies*. Singapore: Springer, 2015. [Online]. Available: https://www.researchgate.net/publication/304195642

[4] G. Q. Luo, Z. F. Hu, L. X. Dong, and L. L. Sun, ''Planar slot antenna backed by substrate integrated waveguide cavity,'' *IEEE Antennas Wireless Propag. Lett.*, vol. 7, pp. 236–239, 2008.

[5] S. Yun, D. Y. Kim, and S. Nam, ''Bandwidth and efficiency enhancement of cavity-backed slot antenna using a substrate removal,'' *IEEE Antennas Wireless Propag. Lett.*, vol. 11, pp. 1458–1461, 2012.

[6] G. Q. Luo, Z. F. Hu, W. J. Li, X. H. Zhang, L. L. Sun, and J. F. Zheng, ''Bandwidth-enhanced low-profile cavity-backed slot antenna by using hybrid SIW cavity modes,'' *IEEE Trans. Antennas Propag.*, vol. 60, no. 4, pp. 1698–1704, Apr. 2012.

[7] M. Mbaye, J. Hautcoeur, L. Talbi, and K. Hettak, ''Bandwidth broadening of dual-slot antenna using substrate integrated waveguide (SIW),'' *IEEE Antennas Wireless Propag. Lett.*, vol. 12, pp. 1169–1171, 2013.

[8] S. Mukherjee, A. Biswas, and K. V. Srivastava, ''Broadband substrate integrated waveguide cavity-backed bow-tie slot antenna,'' *IEEE Antennas Wireless Propag. Lett.*, vol. 13, pp. 1152–1155, 2014.

[9] T. Cheng, W. Jiang, S. Gong, and Y. Yu, ''Broadband SIW cavity-backed modified dumbbell-shaped slot antenna,'' *IEEE Antennas Wireless Propag. Lett.*, vol. 18, no. 5, pp. 936–940, May 2019.

[10] S. Yun, D. Y. Kim, and S. Nam, ''Bandwidth enhancement of cavity-backed slot antenna using a via-hole above the slot,'' *IEEE Antennas Wireless Propag. Lett.*, vol. 11, pp. 1092–1095, 2012.

[11] Y. Shi, J. Liu, and Y. Long, ''Wideband triple- and quad-resonance substrate integrated waveguide cavity-backed slot antennas with shorting vias,'' *IEEE Trans. Antennas Propag.*, vol. 65, no. 11, pp. 5768–5775, Nov. 2017.

[12] Q. Wu, J. Yin, C. Yu, H. Wang, and W. Hong, ''Broadband planar SIW cavity-backed slot antennas aided by unbalanced shorting vias,'' *IEEE Antennas Wireless Propag. Lett.*, vol. 18, no. 2, pp. 363–367, Feb. 2019.

[13] L. Xiang, Y. Zhang, Y. Yu, and W. Hong, ''Characterization and design of wideband penta- and hepta-resonance SIW elliptical cavity-backed slot antennas,'' *IEEE Access*, vol. 8, pp. 111987–111994, 2020.

[14] X. Zhang, T.-Y. Tan, Q.-S. Wu, L. Zhu, S. Zhong, and T. Yuan, ''Pin-loaded patch antenna fed with a dual-mode SIW resonator for bandwidth enhancement and stable high gain,'' *IEEE Antennas Wireless Propag. Lett.*, vol. 20, no. 2, pp. 279–283, Feb. 2021.

[15] A. Iqbal, J. J. Tiang, C. K. Lee, and N. K. Mallat, ''SIW cavity backed self-diplexing tunable antenna,'' *IEEE Trans. Antennas Propag.*, vol. 69, no. 8, pp. 5021–5025, Aug. 2021.

[16] S. K. K. Dash, Q. S. Cheng, R. K. Barik, N. C. Pradhan, and K. S. Subramanian, ''A compact triple-fed high-isolation SIW-based self-triplexing antenna,'' *IEEE Antennas Wireless Propag. Lett.*, vol. 19, no. 5, pp. 766–770, May 2020.

[17] A. Iqbal, J. J. Tiang, S. K. Wong, S. W. Wong, and N. K. Mallat, ''SIW cavity-backed self-quadruplexing antenna for compact RF front ends,'' *IEEE Antennas Wireless Propag. Lett.*, vol. 20, no. 4, pp. 562–566, Apr. 2021.

[18] S. K. K. Dash, Q. S. Cheng, R. K. Barik, F. Jiang, N. C. Pradhan, and K. S. Subramanian, ''A compact SIW cavity-backed self-multiplexing antenna for hexa-band operation,'' *IEEE Trans. Antennas Propag.*, vol. 70, no. 3, pp. 2283–2288, Mar. 2022.

[19] S. A. Razavi and M. H. Neshati, ''Development of a linearly polarized cavity-backed antenna using HMSIW technique,'' *IEEE Antennas Wireless Propag. Lett.*, vol. 11, pp. 1307–1310, 2012.

[20] D. W. Astuti and E. T. Rahardjo, ''Size reduction of cavity backed slot antenna using half mode substrate integrated waveguide structure,'' in *Proc. 4th Int. Conf. Nano Electron. Res. Educ. (ICNERE)*, Nov. 2018, pp. 1–4.

[21] Q. Wu, H. Wang, C. Yu, and W. Hong, ''Low-profile circularly polarized cavity-backed antennas using SIW techniques,'' *IEEE Trans. Antennas Propag.*, vol. 64, no. 7, pp. 2832–2839, Jul. 2016.

[22] D. Chaturvedi, A. Kumar, and S. Raghavan, ''Wideband HMSIW-based slotted antenna for wireless fidelity application,'' *IET Microw., Antennas Propag.*, vol. 13, no. 2, pp. 258–262, Feb. 2019.

[23] D. W. Astuti, M. Asvial, F. Y. Zulkifli, and E. T. Rahardjo, ''Bandwidth enhancement on half-mode substrate integrated waveguide antenna using cavity-backed triangular slot,'' *Int. J. Antennas Propag.*, vol. 2020, pp. 1–9, Dec. 2020.

[24] H. Dashti and M. H. Neshati, ''Development of low-profile patch and semi-circular SIW cavity hybrid antennas,'' *IEEE Trans. Antennas Propag.*, vol. 62, no. 9, pp. 4481–4488, Sep. 2014.

[25] S. Agneessens, ''Coupled eighth-mode substrate integrated waveguide antenna: Small and wideband with high-body antenna isolation,'' *IEEE Access*, vol. 6, pp. 1595–1602, 2018.

[26] J. Zhou and M. Yang, ''A low-profile eighth-mode SIW antenna with dual-sense circular polarization, enhanced bandwidth and simple structure,'' *IEEE Access*, vol. 9, pp. 144375–144384, 2021.

[27] B. Niu and J. Tan, ''Bandwidth enhancement of low-profile SIW cavity antenna using fraction modes,'' *Electron. Lett.*, vol. 55, no. 5, pp. 233–234, Mar. 2019.

[28] O. Caytan, S. Lemey, S. Agneessens, D. V. Ginste, P. Demeester, C. Loss, R. Salvado, and H. Rogier, ''Half-mode substrate-integrated-waveguide cavity-backed slot antenna on cork substrate,'' *IEEE Antennas Wireless Propag. Lett.*, vol. 15, pp. 162–165, 2015.

[29] F. Xu and K. Wu, ''Guided-wave and leakage characteristics of substrate integrated waveguide,'' *IEEE Trans. Microw. Theory Techn.*, vol. 53, no. 1, pp. 66–73, Jan. 2005.

[30] D. M. Pozar, *Microwave Engineering*, 4th ed. Hoboken, NJ, USA: Wiley, 2012.

DIAN WIDI ASTUTI (Member, IEEE) was born in Jakarta, Indonesia. She received the B.Eng. and M.Eng. degrees from Universitas Mercu Buana, Jakarta, and the Ph.D. degree from Universitas Indonesia, Indonesia, in 2022. Since 2012, she has been a Lecturer with the Electromagnetic and Telecommunication Laboratory, Universitas Mercu Buana. Her current research interest includes microwave and millimeter-wave passive component design. She has involved in the 2019 IEEE International Conference on Antenna Measurement Applications (CAMA), Bali, in October 2019, as a Secretary.

YUYU WAHYU was born in Bandung, Indonesia, in February 1962. He received the Ir. degree from the Institut Teknologi Bandung, Bandung, Indonesia, in 1990, the M.Eng. (M.T.) degree in telecommunication information system from the Electrical Engineering Study Program, Institut Teknologi Bandung, in 2000, and the Ph.D. degree in global information and telecommunication studies from the School of Electrical and Informatics Engineering, Institut Teknologi Bandung, in 2010.

He has been with the Telecommunications Research Center, Strategic Electronics, Components and Materials (Telkoma), Indonesian Institute of Sciences, the Research Center for Electronics and Telecommunications, and LIPI, since 1991. He has served as the Head of the Telecommunications and Radio Laboratory, from 2000 to 2003, and in research facilities, from 2010 to 2016. Since 2010, he has been a Lecturer with President University. He has been the Chair of the Research Group of Antennas and Propagation, Research Center for Telecommunication, National Research and Innovation Agency (BRIN), since 2014. Since 2019, he has been appointed as a main researcher of telecommunications transmission. He was involved in a number of activities related to his field of competence, including Guest Research, Okayama, Japan, in 2003, for one and half months, and on the topic of active antenna and radar training at IRCTR-TU, Delft, The Netherlands, in 2006 and 2007. He has been conducting FMCW radar research, since 2006, and electronic support measure (ESM), from 2015 to 2018.

Dr. Wahyu has participated in professional organizations, including as the Head of West Java Province for Himpenindo (Indonesian Researchers Union), from 2020 to 2025, the Indonesian Radar Association, since 2008, and the IEEE Antenna and Propagation Society, since 2010.

FITRI YULI ZULKIFLI (Senior Member, IEEE) received the bachelor's degree in electrical engineering from Universitas Indonesia (UI), in 1997, the M.Sc. degree from the Department of Telecommunication and Information Technology, Karlsruhe Institute of Technology, Germany, in 2002, and the Ph.D. degree in electrical engineering from UI, in 2009.

She joined the Antenna Propagation and Microwave Research Group (AMRG), UI, in 1997. She was the Head of the Telecommunication Laboratory, from 2013 to 2018. She is currently leading the Telecommunication Laboratory and the Department of Electrical Engineering. From 2015 to 2020, she was a Secretary of the Faculty of Engineering Academic Senate. She has been a Lecturer with the Department of Electrical Engineering, Faculty of Engineering, UI, since 1998. Since 2017, she has been a Professor of microwave antenna engineering with the Department of Electrical Engineering. She has published more than 200 papers in international/national journals and conference proceedings. She has been involved in more than 40 granted research. Her research interests include antenna, propagation, microwave, and the field of electromagnetic.

Dr. Zulkifli was assigned as a member of the Professor Council Universitas Indonesia, from 2020 to 2022. She is the Head of the Professional Engineering Study Program, UI. She is involved in many teamwork activities and is also involved in the organizing committees of many seminars and workshops. She has been the Secretary of the IEEE Joint Chapter MTT/AP-S Indonesia. In 2010, she was a Treasurer of the IEEE Joint Chapter MTT/AP-S Indonesia. From 2013 to 2016, she was the Coordinator of technical activity in the IEEE Indonesia Section. She is on the Executive Committee of the Joint Chapter MTT/AP-S and also on the Advisory Board of the IEEE Indonesia Section. In addition, she has been a member of the International Steering Committee (ISC) of the Asia Pacific Microwave Conference (APMC), since 2010, and the International Advisory Board of the International Symposium on Antenna and Propagation (ISAP). From 2019 to 2022, she served as a Committee Member for R10 Conference and Technical Seminar and Conference Quality Management. Due to all her activities, she was a recipient of the Best Lecturer Award (Dosen Berprestasi) from UI and the Best Lecturer Award (4th Place) from the Government of the Republic Indonesia, in 2011. She also received the Deutscher Akademischer Austauschdienst (DAAD) Scholarship for her master's degree in Germany. From 2011 to 2012, she was the Joint Chapter Chair. From 2017 to 2018, she was the IEEE Indonesia Section Chair. She has been the General Chair of the International Conference Quality in Research (QiR), in 2015.

EKO TJIPTO RAHARDJO (Member, IEEE) was born in Pati, Indonesia, in 1958. He received the Ir. degree in electrical engineering from Universitas Indonesia, Depok, Indonesia, in 1981, the M.S. degree in electrical engineering from the University of Hawai'i at Mānoa, Honolulu, HI, USA, in 1987, and the Ph.D. degree in electrical engineering from Saitama University, Urawa, Japan, in 1996.

Since 1982, he has been a Teaching Assistant with the Department of Electrical Engineering, Universitas Indonesia. Since 2005, he has been a Professor of electrical engineering. He was the Chairperson of the University Senate, Universitas Indonesia, from 2011 to 2012; the Head of the Department of Electrical Engineering, Universitas Indonesia, from 2004 to 2008; and the Executive Director of the Quality Undergraduate Education (QUE), Department of Electrical Engineering, Universitas Indonesia, from 1999 to 2004, where he was also the Head of the Telecommunication Laboratory, from 1997 to 2004. Since 2003, he has been the Director of the Antenna Propagation and Microwave Research Group (AMRG), Universitas Indonesia. He has published and presented more than 100 research articles in national and international journals and symposiums. His research interests include antenna engineering, wave propagation, microwave circuits, communication systems, and telecommunications system regulation.

Prof. Rahardjo is a member of the IEEE Antenna and Propagation Society (AP-S) and IEEE Microwave Theory and Technique Society (MTTS). He has been a member of the International Steering Committee (ISC) of the Asia-Pacific Microwave Conference (APMC), since 2010, and the International Advisory Board of the International Symposium on Antenna and Propagation (ISAP), since 2012. He received the Indonesian Government Scholarship through MUCIA, from 1984 to 1987, the Hitachi Scholarship, from 1992 to 1996, the Young Researcher's Award from Universitas Indonesia, in 1996, the second winner of the Best Researcher Award in Science and Technology from Universitas Indonesia, in 2009, and the second winner of the Best Teaching Award from Universitas Indonesia, in 2010. He was the Founder of the IEEE Joint Chapter MTT-S/AP-S, Indonesia. He has served as the President for the IEEE Joint Chapter MTT-S/AP-S, from 2009 to 2010, and the IEEE Indonesia section, from 2014 to 2015. He was the General Chairperson of the Indonesia-Malaysia Microwave and Antenna Conference (IMMAC), Depok, in 2010; the Indonesia-Japan Joint Scientific Symposium (IJJSS), Bali, in 2010; and the General Co-Chairperson of the Indonesia Japan Joint Scientific Symposium (IJJSS), Chiba, Japan, in 2012. In addition, he was the General Chair of the 1st Indonesia–Japan Workshop on Antennas and Wireless Technology (IJAWT), Depok, in 2017, and the 2019 IEEE International Conference on Antenna Measurements and Applications (CAMA), Bali, in October 2019.